JOURNAL OF APPLIED CRYSTALLOGRAPHY

ISSN: 1600-5767
journals.iucr.org/j

In-plane crystalline anisotropy of bulk β-Ga_2O_3

Xiaocui Ma, Rui Xu, Jianfang Xu, Leiying Ying, Yang Mei, Hao Long and Baoping Zhang

J. Appl. Cryst. (2021). **54**, 1153–1157

JOURNAL OF APPLIED CRYSTALLOGRAPHY
ISSN 1600-5767

In-plane crystalline anisotropy of bulk β-Ga_2O_3

Xiaocui Ma,[a] Rui Xu,[a] Jianfang Xu,[b] Leiying Ying,[a] Yang Mei,[a] Hao Long[a]* and Baoping Zhang[a]*

[a]School of Electronic Science and Engineering (National Model Microelectronics College), Xiamen University, Xiamen, Fujian 361005, People's Republic of China, and [b]College of Physical Science and Technology, Xiamen University, Xiamen, Fujian 361005, People's Republic of China. *Correspondence e-mail: longhao@xmu.edu.cn, bzhang@xmu.edu.cn

Received 19 February 2021
Accepted 21 June 2021

Edited by T. J. Sato, Tohoku University, Japan

Keywords: gallium oxide; in-plane anisotropy; X-ray diffraction; Williamson–Hall analysis.

The anisotropy of X-ray diffraction scanning of $(\bar{2}01)$ β-Ga_2O_3 bulk material has been investigated. Symmetric rocking curves (RCs) exhibit distinctly different broadening along different azimuths, with a maximum along [102] and a minimum along a direction rotated by 30° from [010]. Williamson–Hall analysis was applied to study possible factors causing the broadening in these RCs, including instrumental factors, mosaic tilt and coherent scattering. It was found that the RC broadening is determined by both isotropic mosaic tilt and anisotropy in the length over which the crystal structure is not disrupted by limiting factors such as grain boundaries or stacking faults, which we term the 'lateral limited size'. In this case, the lateral limited size is governed by {200} stacking faults along the [102] direction and grain boundaries along the [010] direction. The result presents a new anisotropy characteristic of $(\bar{2}01)$ β-Ga_2O_3.

1. Introduction

In recent years, due to its promising application in power electronics technologies (such as electric vehicles and high-efficiency photovoltaic converters), the ultra-wide-bandgap semiconductor Ga_2O_3 has attracted rapidly increasing attention and been considered as a promising candidate for next-generation high-power electronic devices, solar-blind deep-ultraviolet photodetectors and UV-transparent electrodes (Chen *et al.*, 2019; Pearton *et al.*, 2018). β-Ga_2O_3 is the most stable phase among the five polymorphs [α, β, γ, δ and ε (κ) phases] of Ga_2O_3 under ambient conditions (Playford *et al.*, 2013; Roy *et al.*, 1952). It has a wide band gap (4.4–4.8 eV; Onuma *et al.*, 2015), a high critical breakdown electric field (8 MV cm^{-1}; Higashiwaki *et al.*, 2012) and a very good transparency (>80% transmittance) in the ultraviolet and visible regions (Galazka *et al.*, 2014), and is readily manufacturable via sophisticated growth technologies (Kuramata *et al.*, 2016; Mohamed *et al.*, 2019). Up to now, various growth technologies have been successfully applied in fabricating large β-Ga_2O_3 bulk single crystals and thin films, including edge-defined film-fed growth (EFG), Czochralski and floating zone crystallization, metal–organic vapour phase epitaxy, and mist chemical vapour deposition (von Wenckstern, 2017; Mohamed *et al.*, 2019), of which EFG is the most popular commercialized technology for bulk β-Ga_2O_3 (Kuramata *et al.*, 2016; Guo *et al.*, 2015).

β-Ga_2O_3 belongs to the monoclinic crystalline family. Due to its low symmetry, its thermal conductivity (Guo *et al.*, 2015), electronic band gap (He *et al.*, 2006), optical band gap (Onuma *et al.*, 2015) and crystal structure are characterized by distinct anisotropy. It is known that the macroscopic properties of a material are strongly dependent on its intrinsic microstructure.

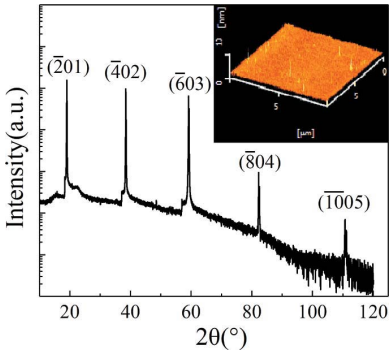

Therefore, fully understanding the anisotropic structure of β-Ga_2O_3 is essential for taking full advantage of its superior physical properties. To date, however, studies of the anisotropy of β-Ga_2O_3 have mainly focused on its optical, thermal and electrical properties. Ueda *et al.* (1997) investigated the anisotropy of the electrical and optical properties of a β-Ga_2O_3 bulk single crystal at room temperature. The conductivity, mobility and absorption edges were different along the [010] and [001] crystallographic directions. Differences in the crystalline and electronic structure along different directions of β-Ga_2O_3 were considered to be the origin of the anisotropy. Yamaguchi (2004) studied the electronic structure of β-Ga_2O_3 using first-principles calculations. The anisotropic optical properties were explained by the selection rule of band-to-band transitions. Guo *et al.* (2015) found a large anisotropy of the thermal conductivities along the [100] and [010] directions at room temperature, and suggested that this was due to differences in the speed of sound. Overall, investigations of the anisotropy of β-Ga_2O_3 have only concentrated on discrepancies in electrical conductivity, thermal diffusivity and luminescence, while the in-plane crystalline anisotropy of β-Ga_2O_3 bulk materials has rarely been mentioned. In contrast, ω-scan broadening anisotropy in non-polar (*a*- or *m*-) and semi-polar GaN films has been reported. McLaurin *et al.* (2008) concluded that basal-plane stacking faults contributed to the peak broadening anisotropy in *m*-plane GaN, using Williamson–Hall analysis of X-ray diffraction (XRD) rocking curves. Moram *et al.* (2009) demonstrated that mosaic tilt was the predominant contribution to the anisotropy of symmetric ω-scan broadening for both *a*- and *m*-plane GaN films.

In this paper, the anisotropic broadening of symmetric rocking curves (RCs) in a bulk $(\bar{2}01)$-oriented β-Ga_2O_3 crystal is investigated. The symmetric RCs exhibit distinctly different half-widths along different in-plane azimuth angles (φ), showing a maximum broadening along [102], a sub-maximum along [010] and a narrowing along the 30° direction. The origin of the anisotropy of the half-widths was studied using Williamson–Hall analysis, considering instrumental, mosaic tilt and coherent scattering factors. The mosaic tilt was confirmed to be isotropic, whereas the characteristic length over which the crystal structure is not disrupted by grain boundaries or stacking faults, which we term the 'lateral limited size', was found to be the predominant cause of the anisotropy of the ω-scan half-widths. This work presents a new viewpoint on the crystallographic anisotropy of β-Ga_2O_3 bulk materials.

2. Experimental details

The sample used in this work was a bulk $(\bar{2}01)$-oriented EFG β-Ga_2O_3 single crystal, purchased from Novel Crystal Technology Inc., Japan. The sample was rectangular in shape ($5 \times 5 \times 0.68$ mm) with a net electron concentration $N_d - N_a \simeq 1 \times 10^{18}$ cm^{-3}. The crystalline structure was characterized using an X-ray diffractometer (PANalytical, X Pert PRO) equipped with Cu $K\alpha_1$ radiation ($\lambda = 1.54$ Å) with a 5×10 mm irradiation area. The signal was detected by a scintillator detector with a 12″ window width. The phases of β-Ga_2O_3 were analysed by 2θ–ω scans. The in-plane crystalline orientations were determined by φ scans of the asymmetric reflections of the $(\bar{4}22)$ plane. The crystalline quality was characterized by ω scans (RCs) along different azimuth angles. The surface morphology was characterized using atomic force microscopy (AFM, Nanonavi, SPA400) in contact scanning mode with a 10×10 μm probing range.

3. Results and discussion

To investigate the crystal structure of bulk β-Ga_2O_3 material, an XRD 2θ–ω scan (phase analysis) was performed, as shown in Fig. 1(*a*). Strong peaks at 2θ = 18.95, 38.40, 59.19, 82.37 and 110.56° correspond to the $\{\bar{2}01\}$ family of planes of β-Ga_2O_3, which indicates that the samples are dominated by the monocrystalline β-Ga_2O_3 phase. The surface morphology of the β-Ga_2O_3 bulk material was characterized by AFM, with an r.m.s. roughness of 0.32 nm, showing atomic flatness. The superior r.m.s. value and sharp peaks confirm the good crystalline quality.

The crystal symmetry of β-Ga_2O_3 was also characterized by φ scans of the asymmetric $(\bar{4}22)$ plane, as shown in Fig. 1(*b*). Only two diffraction peaks separated by 180° were detected, due to the natural monoclinic structure of β-Ga_2O_3. The asymmetric scanning does not show sixfold symmetry with a 60° interval, which has often been observed in thin films deposited on sapphire (Ghose *et al.*, 2017) or GaN (Cao *et al.*, 2018). This confirms the pure single-crystalline nature of this EFG sample, rather than the six twin crystals seen in heteroepitaxial thin films. Owing to the low symmetry of the β-Ga_2O_3 crystal, significant in-plane anisotropy of properties such as thermal and electrical conductivity occurs (Guo *et al.*, 2015; Ueda *et al.*, 1997; Wong *et al.*, 2016). Moreover, due to the anisotropy of the atomic binding energy and chemical potential, microscopic parameters (such as dislocations, stacking faults and grains) are also expected to exhibit different character along different in-plane directions.

The X-ray RCs of the symmetric $(\bar{6}03)$, $(\bar{8}04)$ and $(\bar{10}05)$ reflections were measured along various in-plane azimuths. Typical $(\bar{10}05)$ RCs along [102] (labelled 90°), [010] (labelled 0°) and 30° are shown in Fig. 2(*a*). The full widths of the RCs vary in the different directions, being 140.01 and 96.84″ when

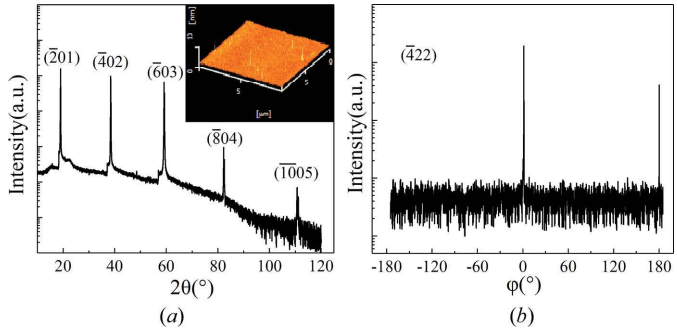

Figure 1
(*a*) An X-ray 2θ–ω scan of bulk β-Ga_2O_3, with a 10×10 μm AFM surface image inset. (*b*) A φ scan of the $(\bar{4}22)$ plane of bulk β-Ga_2O_3.

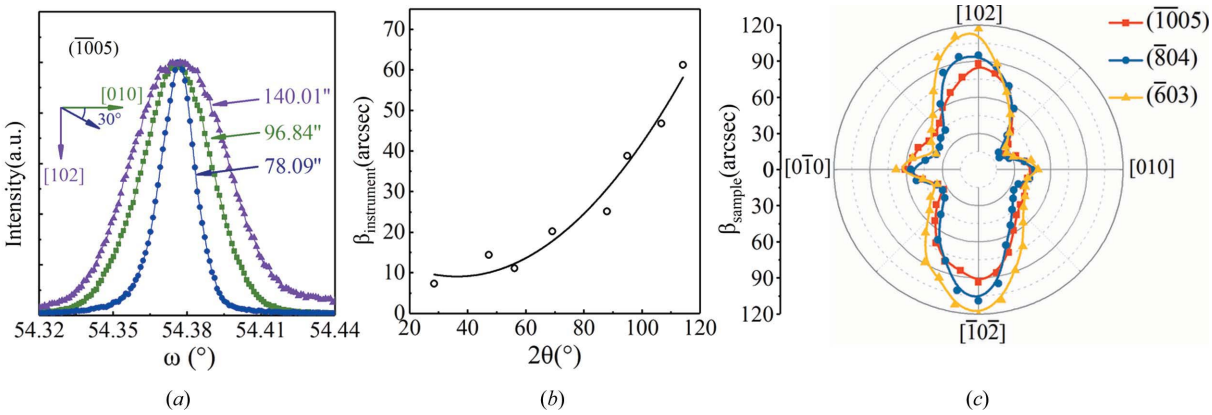

Figure 2
(*a*) Rocking curves of the β-Ga_2O_3 ($\bar{1}005$) reflection at azimuths of 0, 30 and 90° before calibration for instrumental broadening. (*b*) Instrumental broadening plotted versus 2θ for this work. (*c*) A polar diagram of sample broadening of the ($\bar{1}005$), ($\bar{8}04$) and ($\bar{6}03$) reflections along different azimuths.

the X-rays are aligned with the [102] and [010] directions, respectively, and only 78.09″ at the azimuth of the 30° direction.

In X-ray diffraction, RC broadening consists of instrumental broadening and sample broadening ($\beta = \beta_{\rm instrument} + \beta_{\rm sample}$). The instrumental broadening arises from two factors: (i) the optical modules (such as X-ray sources, slits, detector windows *etc.*) inevitably have a nonzero size, which contributes to peak broadening by the size effect; (ii) the X-ray wavelength inevitably has a certain broadening distribution centred on Cu $K\alpha$ λ = 1.54 Å. This incoherent X-radiation could increase the instrumental broadening. Since the crystal quality of our bulk β-Ga_2O_3 was very good with an extremely low measured width (only a few tens of arcseconds), $\beta_{\rm instrument}$ becomes non-negligible. Therefore, $\beta_{\rm instrument}$ was removed before further analysis. A standard Si(100) wafer was used to derive $\beta_{\rm instrument}$ for the X-ray diffractometer, as depicted in Fig. 2(*b*). The value of $\beta_{\rm instrument}$ increases with diffraction angle. After subtracting $\beta_{\rm instrument}$, we obtain Fig. 2(*c*), which shows a polar diagram of $\beta_{\rm sample}$ for the ($\bar{1}005$), ($\bar{8}04$) and ($\bar{6}03$) reflections along different azimuths. In contrast to the asymmetric scanning results in Fig. 1(*b*), a modified twofold symmetric anisotropy is present in all three symmetric planes. However, along the [102] and [010] directions, the ω-scan widths reach a maximum and sub-maximum, respectively. The minimum width is at the azimuth of the 30° direction. Anisotropy of a crystal structure and of quality seriously affect the structural design and performance of a device, so clarifying the intrinsic mechanism of the β-Ga_2O_3 bulk broadening anisotropy is necessary.

In XRD measurements, the sample broadening of an ω scan arises from the superimposition of various broadening factors (Moram *et al.*, 2009), including mosaic tilt or twist, macrostrain, and the characteristic length over which the crystal structure is not disrupted by grain boundaries or stacking faults, which we term 'lateral limited size'. Microstrain broadening has no effect on symmetric diffraction, since the diffraction detects no lateral component. Mosaic twist induced by edge dislocations also does not distort the vertical structure of a symmetric plane since their Burgers vectors lie inside the planes. Therefore, in this work, the $\beta_{\rm sample}$ value for symmetric diffraction was taken to be the sum of the contributions of the mosaic tilt (caused by screw dislocations) and lateral limited size (caused by stacking faults and grain boundaries vertical to the surface), assuming Lorentzian peak shapes (Metzger *et al.*, 1998; Williamson & Hall, 1953):

$$\beta_{\rm sample} = \beta_{\rm tilt} + \beta_{\rm L} = \beta_{\rm tilt} + \frac{\lambda}{2L\sin\theta}, \qquad (1)$$

where $\beta_{\rm sample}$ is the measured sample broadening, $\beta_{\rm tilt}$ is the broadening due to mosaic tilt, $\beta_{\rm L}$ is the broadening due to lateral limited size (L), λ is the incident X-ray wavelength and θ is the Bragg angle. Fig. 3(*a*) illustrates the broadening caused by mosaic tilt and lateral limited size in reciprocal space. The experimental angular broadening ($\beta_{\rm tilt}$) induced by mosaic tilt is constant with X-ray diffraction vector **S**,

$$|\mathbf{S}| = \frac{2\pi}{d} = \frac{4\pi}{\lambda}\sin\theta, \qquad (2)$$

(Moram & Vickers, 2009). In reciprocal space, the mosaic tilt broadening is expressed as $S\beta_{\rm tilt}$, which increases linearly with

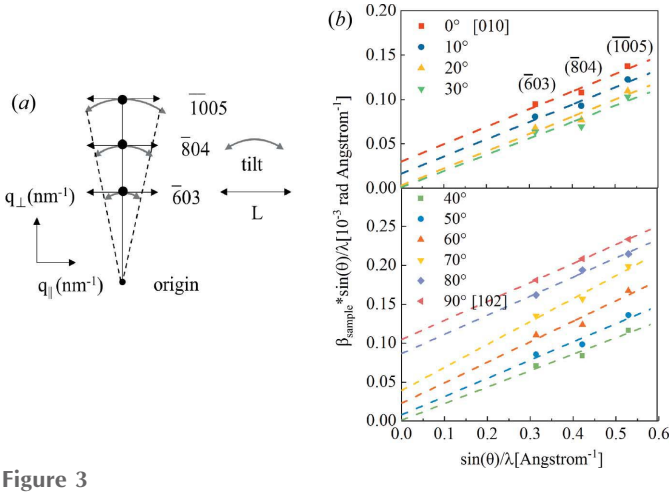

Figure 3
(*a*) A schematic diagram of the broadening caused by mosaic tilt and lateral limited size in reciprocal space. (*b*) A Williamson-Hall plot for bulk ($\bar{2}01$) β-Ga_2O_3 along azimuth angles in the range 0–90°.

S, whereas the lateral broadening $S\beta_L$ stays constant in reciprocal space and the experimental angular values β_L change with diffraction vector **S**

Williamson–Hall (W-H) analysis is a theoretical method to investigate X-ray diffraction broadening of crystalline plane groups (Williamson & Hall, 1953). A W-H curve is plotted as $(\beta_{sample}\sin\theta)/\lambda$ versus $\sin\theta/\lambda$:

$$\frac{\beta_{sample}\sin\theta}{\lambda} = \frac{\beta_{tilt}\sin\theta}{\lambda} + \frac{1}{2L}. \quad (3)$$

The values of β_{tilt} and $1/2L$ can be derived from the slope and intercept of the fitting line. ω scans of the $(\bar{6}03)$, $(\bar{8}04)$ and $(\bar{1}0\bar{1}005)$ reflections along the 0–90° azimuth range are fitted by W-H curves in Fig. 3(*b*). All the fitted lines are nearly parallel, indicating that the mosaic tilt broadening is nearly isotropic and stays constant along the various azimuths. On the other hand, the intercepts $1/2L$ vary significantly at different azimuths, decreasing first from 0.03 mrad Å^{-1} for the [010] (0°) direction to nearly zero at 30°, and then recovering to a maximum exceeding 0.1 mrad Å^{-1} for the [102] (90°) direction. This variation in the intercept and invariability of the slope (β_{tilt}) confirms that the lateral limited size, rather than the mosaic tilt, is of an anisotropic nature in β-Ga_2O_3.

Utilizing the equation $\rho_{screw} = \beta_{tilt}^2/(4.35\mathbf{b}^2)$ (Metzger *et al.*, 1998), where **b** is the Burgers vector of the screw dislocation, the screw dislocation density ρ_{screw} can be estimated as roughly 3×10^6 to 4×10^6 cm^{-2}, which is approximately uniformly distributed within the plane. Since the sample used in this work was doped ($N_d - N_a \simeq 1\times10^{18}$ cm^{-3}), the estimated screw dislocation density was larger than that reported for non-doped EFG β-Ga_2O_3 (Yao *et al.*, 2019, 2020).

Note, however, that different β_L appear along various in-plane directions, showing different lengths L along the various azimuth angles. Previously, Gao *et al.* (2018) and Wu *et al.* (2019) observed (200) plane stacking faults in $(\bar{2}01)$ β-Ga_2O_3 bulk material using high-resolution transmission electron microscopy [the blue planes illustrated in Fig. 4(*c*)]. The (200) stacking faults induce coherent scattering and cause RC broadening when the X-rays are incident from the [102] direction. The (200) stacking-fault density was estimated to be 2.09×10^4 cm^{-1} using the value of $1/2L$ obtained from the W-H fit along the [102] direction. Up to now, there has been no report on the existence of stacking faults parallel to the [102] direction in β-Ga_2O_3. Therefore, we speculate that the lateral limited size measured along the [010] direction is related to grain boundaries. An average grain size of 1.67 µm was obtained using the value of $1/2L$ obtained from the W-H fit along the [010] direction.

Fig. 4(*b*) shows the contribution of the mosaic tilt broadening and lateral size broadening along each azimuth direction. It can be seen that the mosaic tilt broadening always dominates the sample broadening and is nearly isotropic. In contrast, the contribution from the lateral limited size due to stacking faults and grain boundaries is anisotropic, which contributes to the anisotropy of β_{sample}.

The anisotropy in the bulk β-Ga_2O_3 ω-scan half-width originates from the nucleation kinetics of defects. During crystal growth, excess strain energy is relieved through the lattice relaxation process, inevitably generating defects. Defects are more easily formed along the direction of lower formation energy. There are two types of Ga–O structural cell in β-Ga_2O_3, tetrahedral GaO_4 and octahedral GaO_6, which are stacked layer by layer. Gallium vacancies are always distributed along the [010] direction between the GaO_6 units (Yamaguchi & Kuramata, 2018). The elastic stress field of dislocation could be efficiently reduced by this vacancy array. Therefore, the formation energy of dislocations along the [010] direction will be reduced, enhancing the probability of dislocation generation. It has been demonstrated by chemical etching and X-ray topography that stacking faults are associated with a partial dislocation loop (Yamaguchi & Kuramata, 2018; Yao *et al.*, 2019; Masuya *et al.*, 2019), indicating that the vectors of the stacking fault are identical to the Burgers vector of the partial dislocation loop. Our work has shown that the

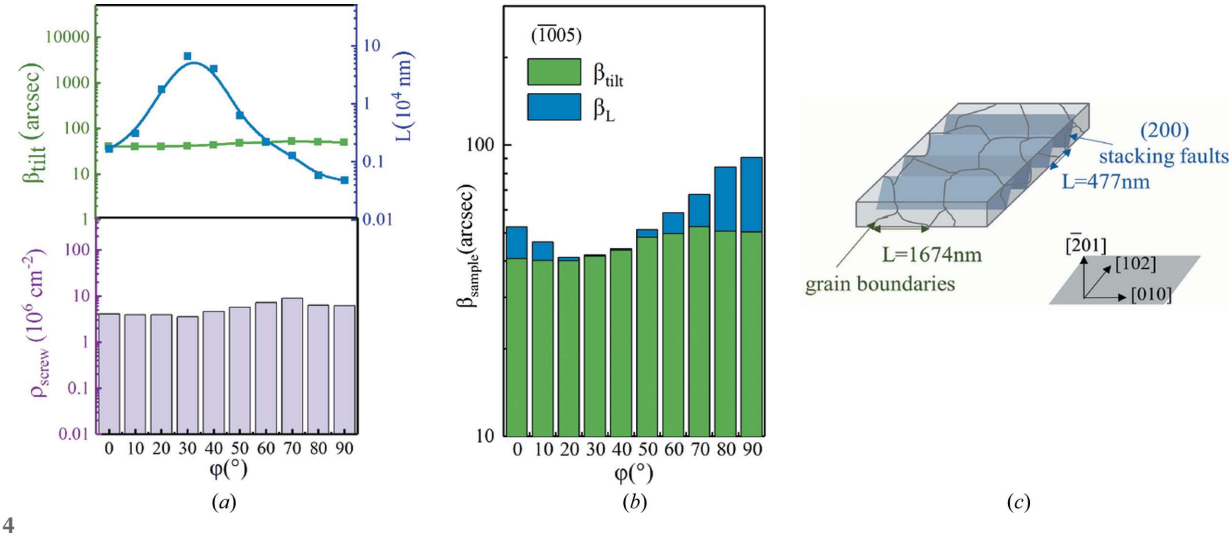

Figure 4
(*a*) The variation in L, β_{tilt} and ρ_{screw} with azimuth angle. (*b*) The contribution of the tilt broadening and lateral broadening to sample broadening in bulk $(\bar{2}01)$ β-Ga_2O_3. (*c*) A schematic diagram of the lateral limited size distribution in bulk $(\bar{2}01)$ β-Ga_2O_3.

greater probability of (100) stacking faults corresponds to the smaller lateral limited size measured in the [102] direction.

4. Conclusions

The anisotropy of the β-Ga_2O_3 symmetric ω scan has been investigated. The half-widths were characterized by a modified twofold symmetric anisotropy, reaching a maximum and a minimum along the [102] direction and at 30° to the [010] direction, respectively. Williamson–Hall analysis of rocking curves revealed that the mosaic tilt due to screw dislocations contributed isotropically, while the lateral limited size, determined by stacking faults and grain boundaries, induces anisotropic ω-scan broadening.

Funding information

The following funding is acknowledged: National Key Research and Development Program of China (grant Nos. 2017YFE0131500 and 2016YFB0400803); Natural Science Foundation of Fujian Province of China (grant No. 2019J05023); Youth Innovation Foundation of Xiamen, China (grant No. 3502Z20206055).

References

Cao, Q., He, L., Xiao, H., Feng, X., Lv, Y. & Ma, J. (2018). *Mater. Sci. Semicond. Process.* **77**, 58–63.
Chen, X., Ren, F., Gu, S. & Ye, J. (2019). *Photon. Res.* **7**, 381–415.
Galazka, Z., Irmscher, K., Uecker, R., Bertram, R., Pietsch, M., Kwasniewski, A., Naumann, M., Schulz, T., Schewski, R., Klimm, D. & Bickermann, M. (2014). *J. Cryst. Growth*, **404**, 184–191.
Gao, S., Wu, Y., Kang, R. & Huang, H. (2018). *Mater. Sci. Semicond. Process.* **79**, 165–170.
Ghose, S., Rahman, S., Hong, L., Rojas-Ramirez, J. S., Jin, H., Park, K., Klie, R. & Droopad, R. (2017). *J. Appl. Phys.* **122**, 095302.
Guo, Z., Verma, A., Wu, X., Sun, F., Hickman, A., Masui, T., Kuramata, A., Higashiwaki, M., Jena, D. & Luo, T. (2015). *Appl. Phys. Lett.* **106**, 111909.
He, H., Orlando, R., Blanco, M. A., Pandey, R., Amzallag, E., Baraille, I. & Rérat, M. (2006). *Phys. Rev. B*, **74**, 195123.
Higashiwaki, M., Sasaki, K., Kuramata, A., Masui, T. & Yamakoshi, S. (2012). *Appl. Phys. Lett.* **100**, 013504.
Kuramata, A., Koshi, K., Watanabe, S., Yamaoka, Y., Masui, T. & Yamakoshi, S. (2016). *Jpn. J. Appl. Phys.* **55**, 1202A2.
Masuya, S., Sasaki, K., Kuramata, A., Yamakoshi, S., Ueda, O. & Kasu, M. (2019). *Jpn. J. Appl. Phys.* **58**, 055501.
McLaurin, M. B., Hirai, A., Young, E., Wu, F. & Speck, J. S. (2008). *Jpn. J. Appl. Phys.* **47**, 5429–5431.
Metzger, T., Höpler, R., Born, E., Ambacher, O., Stutzmann, M., Stömmer, R., Schuster, M., Göbel, H., Christiansen, S., Albrecht, M. & Strunk, H. P. (1998). *Philos. Mag. A*, **77**, 1013–1025.
Mohamed, H. F., Xia, C., Sai, Q., Cui, H., Pan, M. & Qi, H. (2019). *J. Semiconductors*, **40**, 011801.
Moram, M. A., Johnston, C. F., Hollander, J. L., Kappers, M. J. & Humphreys, C. J. (2009). *J. Appl. Phys.* **105**, 113501.
Moram, M. A. & Vickers, M. E. (2009). *Rep. Prog. Phys.* **72**, 036502.
Onuma, T., Saito, S., Sasaki, K., Masui, T., Yamaguchi, T., Honda, T. & Higashiwaki, M. (2015). *Jpn. J. Appl. Phys.* **54**, 112601.
Pearton, S. J., Yang, J., Cary, P. H., IV, , Ren, F., Kim, J., Tadjer, M. J. & Mastro, M. A. (2018). *Appl. Phys. Rev.* **5**, 011301.
Playford, H. Y., Hannon, A. C., Barney, E. R. & Walton, R. I. (2013). *Chem. Eur. J.* **19**, 2803–2813.
Roy, R., Hill, V. G. & Osborn, E. F. (1952). *J. Am. Chem. Soc.* **74**, 719–722.
Ueda, N., Hosono, H., Waseda, R. & Kawazoe, H. (1997). *Appl. Phys. Lett.* **71**, 933–935.
Wenckstern, H. von (2017). *Adv. Electron. Mater.* **3**, 1600350.
Williamson, G. K. & Hall, W. H. (1953). *Acta Metall.* **1**, 22–31.
Wong, M. H., Sasaki, K., Kuramata, A., Yamakoshi, S. & Higashiwaki, M. (2016). *Jpn. J. Appl. Phys.* **55**, 1202B9.
Wu, Y. Q., Gao, S., Kang, R. K. & Huang, H. (2019). *J. Mater. Sci.* **54**, 1958–1966.
Yamaguchi, H. & Kuramata, A. (2018). *J. Appl. Cryst.* **51**, 1372–1377.
Yamaguchi, K. (2004). *Solid State Commun.* **131**, 739–744.
Yao, Y., Ishikawa, Y. & Sugawara, Y. (2019). *Phys. Status Solidi A*, **217**, 1900630.
Yao, Y., Sugawara, Y. & Ishikawa, Y. (2020). *J. Appl. Phys.* **127**, 205110.